Vainio, Valtteri; Majuri, Jaakko; Haverinen, Petteri; Miettinen, Mikael; Viitala, Raine

Aerostatic bearing for large rotor

Published in:
Engineering for a changing world: Proceedings : 60th ISC, Ilmenau Scientific Colloquium, Technische Universität Ilmenau, September 04-08, 2023

DOI:
10.22032/dbt.58845

Published: 01/11/2023

Document Version
Publisher's PDF, also known as Version of record

Please cite the original version:
Vainio, V., Majuri, J., Haverinen, P., Miettinen, M., & Viitala, R. (2023). Aerostatic bearing for large rotor. In K.-U. Sattler (Ed.), *Engineering for a changing world: Proceedings : 60th ISC, Ilmenau Scientific Colloquium, Technische Universität Ilmenau, September 04-08, 2023* Universitatsverlag Ilmenau. https://doi.org/10.22032/dbt.58845

Article Identifier
DOI: 10.22032/dbt.58845
URN: urn:nbn:de:gbv:ilm1-2023isc-107:8

60th ILMENAU SCIENTIFIC COLLOQUIUM Technische Universität Ilmenau, 4 – 8 September 2023
URN: urn:nbn:de:gbv:ilm1-2023isc:1

AEROSTATIC BEARING FOR LARGE ROTOR

Valtteri Vainio [1], Jaakko Majuri [1], Petteri Haverinen[1], Mikael Miettinen [1], Raine Viitala [1]

[1] Mechatronics Group, Aalto University, Espoo, Finland

ABSTRACT

In cardboard and paper manufacturing, the paper web is handled with large scale rolls. From the machine design point of view, those rolls are large rotors with high stiffness, accuracy and balance requirements. In paper machines, the rotors not only guide the web but also are used to perform different treatments for the manufactured product.

In the cases where highest load and straightness is required, deflection compensated rolls are applied. Commonly, deflection compensated paper machine rolls consist of stationary axle in the middle of the roll and hydrostatically supported rotating shell. Main downside of the traditional deflection compensated roll is high energy consumption. High friction occurs in the hydrostatic system supporting the rotating shell.

In this research, test device was built to perform conceptual investigation of suitability of aerostatic bearings to be applied in the deflection compensated rolls. Porous material aerostatic bearing was built in concave shape to interact with the shell of a roll. The bearing design was a combination of a bearing and a sealed chamber restricted with the bearing itself from the ambient. Air consumption, load and drive motor current were measured at various rotating speeds.

The results of the research show the performance of the investigated bearing at various operating parameters, from which the point of highest performance can be determined. The results suggest that the porous material based aerostatic bearings as a technology is feasible to be applied in the deflection compensation systems. The validation of the feasibility of the concept of the aerostatic deflection compensation enables further investigations into optimizing the performance of the system for widespread utilisation.

Index Terms - Aerostatic bearing, deflection compensation, Rotor dynamics, Tribology

INTRODUCTION

Large scale rotors are widely used in industry, for example in paper machinery and steel mills. In paper machinery rotors are used to guide the paper web and also to perform finishing treatments for the product. Loads carried with the rotors are large which furthermore defines high stiffness and load carrying requirements for the system. Calendering is a paper treating method which results shiny surface for the paper. In calandering, a paper web is lead through a roll nip, which consists of two or several rolls located with axial alignment. Gap between rolls equals with paper thickness and therefore variations in the gap causes thickness variation to the product. Line load between the rolls may reach 1000 tons per meter and acceptable paper thickness variation is in micrometer scale. Length of the roll in modern paper machine is commonly over 10 meters. Moreover, these operating conditions and strict limitations for the deflection of the rolls results major challenges in the machine designing. [1]

State-of-the-art solution to overcome with the high line loads is to utilize deflection compensation system inside of the roll. Deflection compensation system consists of hydraulic systems, located inside of the roll, which hydrostatically supports the roll shell and thus compensates the deflection and retains the gap for paper equal along the nip contact. Energy consumption in these hydrostatic systems is major which furthermore motivates the development of new and more efficient systems.

Aerostatic bearings are commonly used in high precision devices and applications in heavy machinery are relatively rare [2,3]. Target of this research was to investigate the conceptual suitability of porous material aerostatic bearings to be used in deflection compensation systems. The present study builds upon a previous study that investigated a planar bearing with a similar structure [4], while the present study investigates a curved bearing acting against a roll. Almost frictionless operation of aerostatic bearing is the main motivation to apply them in paper machines.

MATERIAL AND METHODS

A test bench located at Aalto University ARotor laboratory was used as a base for the experiments. Over the rotor, a frame for supporting the investigated bearing was manufactured and assembled. The frame featured a four bar linkage mechanism for moving the aerostatic bearing used in the measurements. Force sensors to measure the load of the bearing were located between the bearing and the frame. The sensors were calibrated with known weights before installation. Test bench layout is presented in Figure 1.

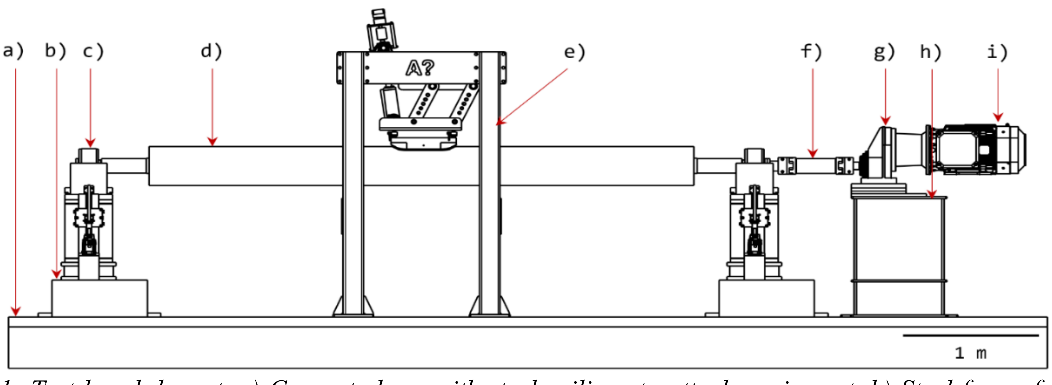

Figure 1: Test bench layout. a) Concrete base with steel railings to attach equipment, b) Steel frame for rotor bearing assembly, c) Rotor bearing assembly, d) Rotor, e) Support structure for the studied bearing, f) Flexible coupling, g) Gearbox, h) Steel base to support motor and gearbox, and i) Motor used to rotate rotor.

The constructed support structure for the bearing has been presented by Majuri et. al. [5] The structure features four bar linkage mechanism to drive bearing attachment cradle. This enables vertical positioning of the bearing in relation to the rotor. For the movement, a servo motor with brake and planetary gearbox was used to rotate a ball screw. A ball screw nut was secured to the cradle, thus whilst the screw rotates, the nut moves on the screw and simultaneously moves the cradle. The cradle had mounting holes for four force sensors, to which the bearing frame was attached. Figure 2 presents the support structure and its components.

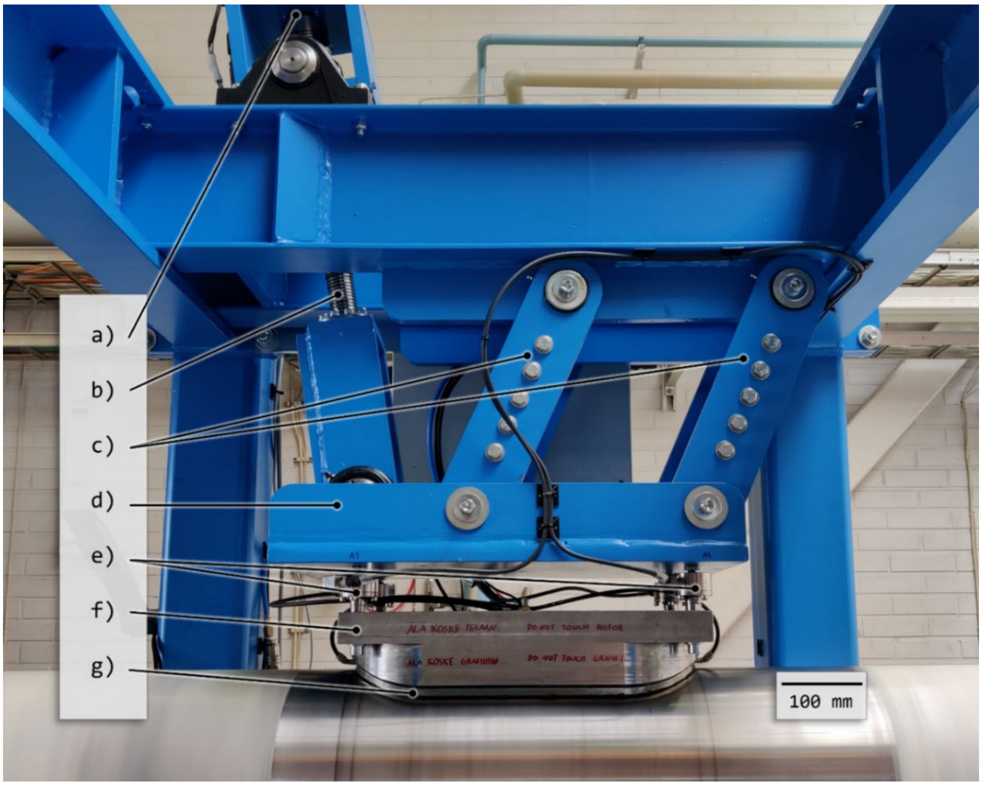

Figure 2: Device for moving the bearing. a) Servomotor with brake and planetary gearbox, b) Ball screw, c) Four bar linkage mechanism reaction arms, d) Cradle to attach linkage, ball screw and force sensors, e) Force sensors, f) Bearing frame, and g) Bearing seal

A concave aerostatic bearing was manufactured. The bearing consisted of a pressure volume, which was isolated from ambient with an aerostatic seal. The seal consisted of porous graphite, which was glued with epoxy to an aluminium seat, referred to as a gum. The gum was attached to the bearing frame with multiple plate springs. The frame was a monolithic steel structure that featured a groove to which a preload tube was added. The preload tube was glued to the bottom of the groove of the bearing frame, and to the top surface of the aluminium gum. The gluing ensures that pressure will not escape the chamber between bearing seal and frame. Figure 3 presents the cross-sectional structure of the bearing, flexible support mechanism and preload tube. The seal of the bearing was ground in-situ to mate the shape of the seal graphite to the shape of the rotor surface. First, rough grain abrasive was used to remove excess material and make graphite surface curved. Then, a finer abrasive film with a grain size of 9 microns was used to improve surface of the graphite. Figure 5 presents the ground bearing surface. To feed air to the bearing, pneumatic system was designed and manufactured. Pressure regulators were used to adjust pressures of the system, whilst a set of flow and pressure sensors were used to measure system parameters. Pneumatic system is presented in Figure 4. The rotor of the test bench was prepared as well. Surface of the rotor was grinded to achieve roundness 10 microns. Additionally, the rotor had some small surface defections with sharp edges. To prevent damage of the graphite, sharp edges and burrs were removed with flat grinding stones.

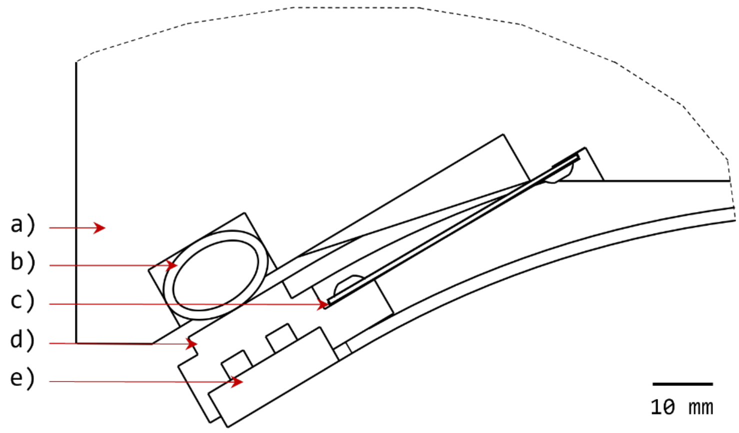

Figure 3: Aerostatic bearing cut section. a) Bearing frame, b) Preload tube, c) Plate spring, d) Aluminium gum, and e) Graphite restrictor.

The particular rotor has been well studied. It has different natural frequencies in horizontal and vertical direction due to the differences in the stiffnesses of the support. The horizontal natural frequency is approximately 21.6 Hz and the vertical natural frequency is approximately 30 Hz [6]. The rotor had a rather large residual unbalance during the tests in order to provide a harsh test environment for the aerostatic bearing. Unbalances at the rotor ends were G 2 and G 12, which contribute to large vibration amplitudes at subcritical resonances of the rotor. To evaluate contact of the rotor and the bearing seal, rotor drive motor current was measured.

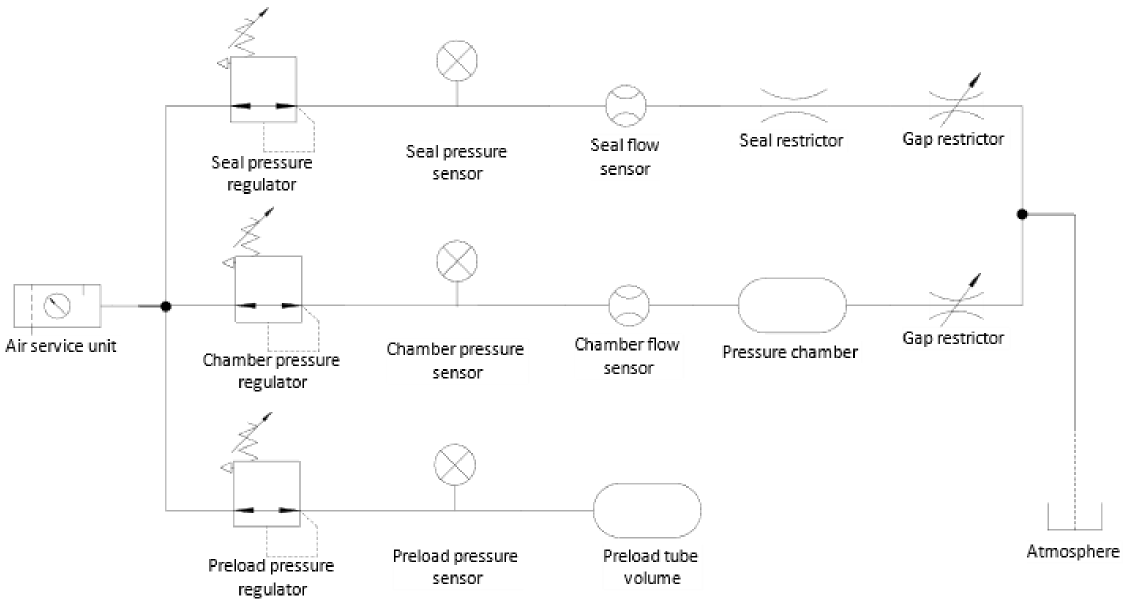

Figure 4: Pneumatic system of the test setup. Regulator were controlled with analogue voltage signal.

For comparing the measurement results between altering measurement points, the authors suggested using a performance index. Best bearing performance is essentially achieved at such seal and chamber pressure combination, at which there is the largest reaction force with lowest increase in motor current and lowest usage of air. Therefore, it was suggested that measurement results are normalized between 0, 1 and following equation used to calculate performance index:

$$PI = F_t - (0.25\, Q_{seal} + 0.25\, Q_{chamber} + 0.5\, I_{motor})$$

Where PI is performance index, F_t is total bearing force, Q_{seal} and $Q_{chamber}$ are air consumptions of the seal and the chamber, and finally I_{motor} is the motor current increase compared to a freely rotating rotor.

Figure 5: Porous material aerostatic bearing is forming a chamber restricted from ambient.

RESULTS

Performance measurements for the bearing were made with altering rotor rotational frequency from 4 Hz to 10 Hz in 1 Hz increments. At each frequency, bearing seal preload pressure was altered from 0 to 0.38 MPa, while bearing pressure chamber pressure was altered from 0 to 0.18 MPa. Bearing seal supply pressure was kept constant at 0.6 MPa. In order to distinguish contact situations, the rotor motor current was measured first without any load, i.e., with the investigated bearing far away from the rotor. Subsequently, the motor current under load was compared to the unloaded condition to determine the difference. High motor current difference indicates contact. Figure 6 presents bearing performance characteristics at 4 Hz, from top left with total bearing force, motor current difference, chamber air consumption and seal air consumption. Horizontal axes feature measured chamber pressure and vertical axes preload pressure. Figures 7 and 8 feature same measured parameters, but with 7 Hz and 9 Hz rotational frequencies. Table 1 presents the results of the operating point with the best performance index at each rotational frequency.

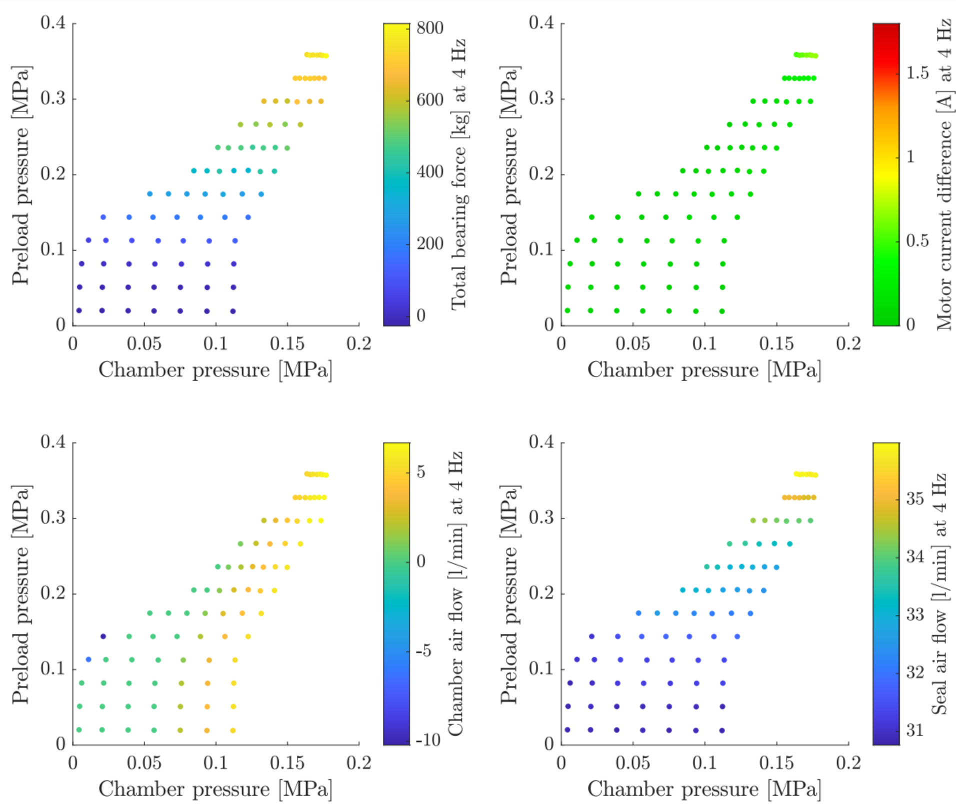
Preload pressure [MPa]
Chamber pressure [MPa]
Total bearing force [kg] at 4 Hz
Motor current difference [A] at 4 Hz
Chamber air flow [l/min] at 4 Hz
Seal air flow [l/min] at 4 Hz

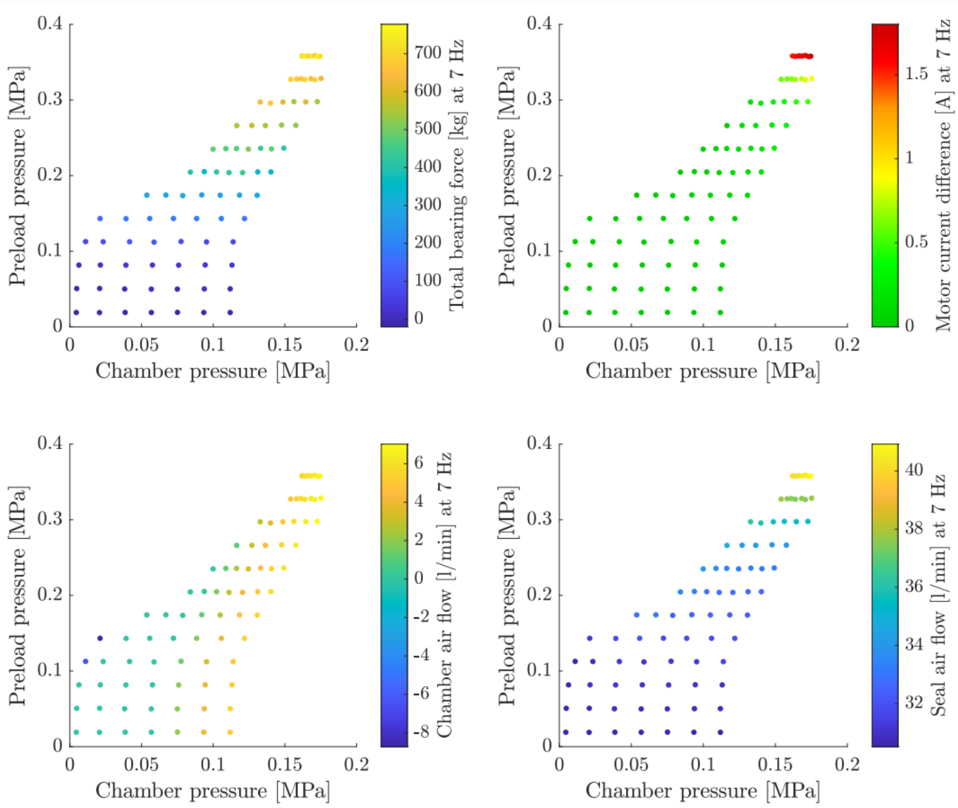
Preload pressure [MPa]
Chamber pressure [MPa]
Total bearing force [kg] at 7 Hz
Motor current difference [A] at 7 Hz
Chamber air flow [l/min] at 7 Hz
Seal air flow [l/min] at 7 Hz

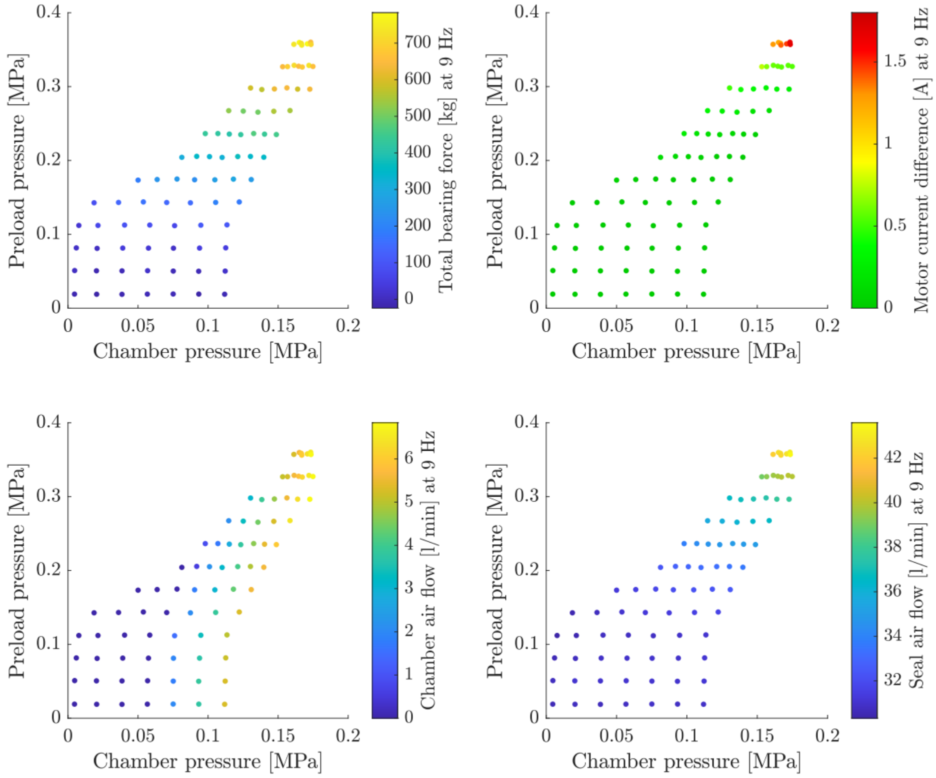
Preload pressure [MPa]
Chamber pressure [MPa]
Total bearing force [kg] at 9 Hz
Motor current difference [A] at 9 Hz
Chamber air flow [l/min] at 9 Hz
Seal air flow [l/min] at 9 Hz

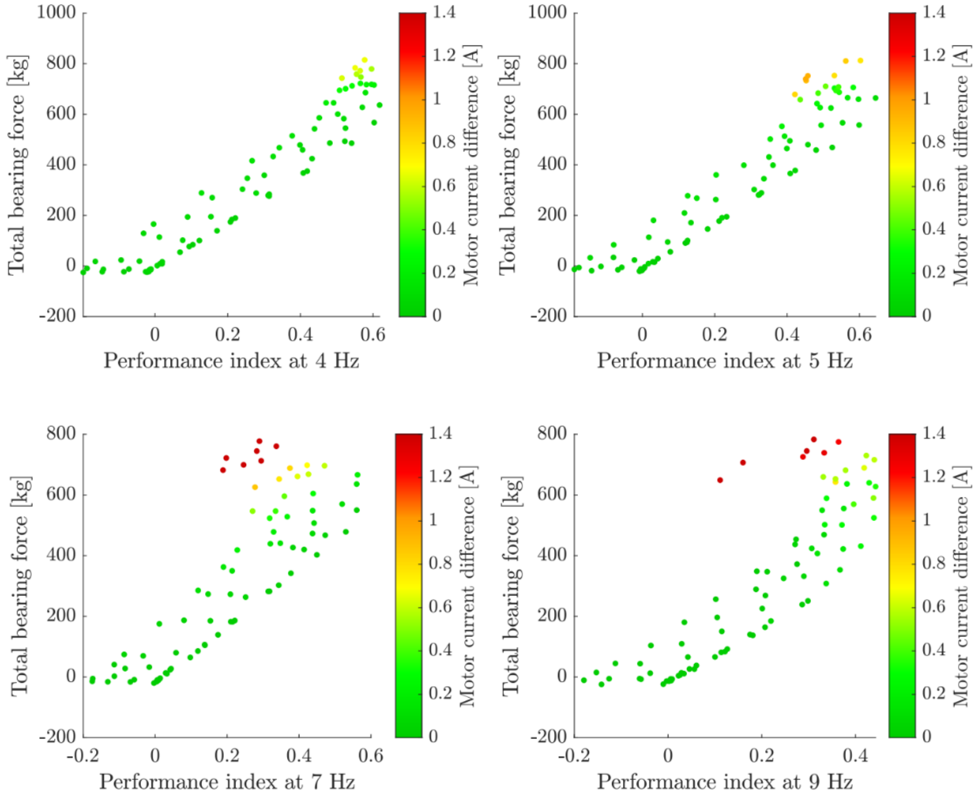
Total bearing force [kg]
Motor current difference [A]
Performance index at 4 Hz
Performance index at 5 Hz
Performance index at 7 Hz
Performance index at 9 Hz

Table 1: The performance parameters at the point with the best performance index at each rotational frequency.

Parameter	4 Hz	5 Hz	6 Hz	7 Hz	8 Hz	9 Hz	10 Hz
Performance index	0.62	0.64	0.62	0.56	0.58	0.44	0.22
Total force [kg]	636	664	688	666	668	627	600
Seal air flow [l/min]	34.4	34.4	34.8	36.0	38.7	37.2	42.7
Chamber air flow [l/min]	2.37	2.51	3.63	3.70	2.51	4.72	4.00
Motor current difference [A]	0.09	0.10	0.13	0.22	0.09	0.34	1.19
Chamber pressure [Mpa]	0.13	0.13	0.14	0.14	0.13	0.15	0.14
Preload pressure [Mpa]	0.30	0.30	0.30	0.30	0.30	0.30	0.30

DISCUSSION

Results of the measurements demonstrate that such pressures for operating the bearing can be found, at which it carries a load without notable increase in the friction between the rotor and the bearing. Furthermore, the best performing parameters (Table 1) are consistent across all rotational frequencies used in the study. The best performance is achieved with 0.3 MPa preload pressure and 0.14 MPa chamber pressure, with which bearing reaction force is measured as approximately 650 kg. With the parameters, motor current differs from one rotational frequency to another, but stays rather low in every one of them, except 10 Hz. Coincidentally, 10 Hz rotational frequency is close to both vertical and horizontal subcritical frequency of the rotor. Therefore, vibrations of the rotor at that point have been large amplitude and multi-directional. It is assumed that bearing is especially susceptible to horizontal vibrations of the rotor, as those move the bearing seal to a direction which is not designed to move much.

The results presented in Figures 6-8 indicate clear consistency between the different operational points. Motor current increases simultaneously with increased bearing load. Furthermore, this means that the system seems to have less load carrying capacity at higher rotational speeds. The authors suggest that the reason may be that the roll surface carries air from bearing air gap and thus decreases the load carrying capacity. The air carried by the surface may also be the reason for the observed decrease in chamber air flow at higher rotational speeds. The chamber air flow is decreased especially at lower preload pressures. At higher preload pressures, the bearing air gap is probably smaller and thus the roll surface carries less air.

The friction of the investigated bearing was measured from the current of the drive motor of the roll. The method is simple; however, it has some uncertainties. As the roll is supported from it ends by conventional roller bearings, the increased load on the roll leads to increased friction in the bearings. This friction effect cannot be separated from the friction of the friction of the investigated air bearing. Thus, the contact determination is more qualitative than quantitative. In further studies, the friction will be measured with an intermediate structure on the bearing support frame. Force sensors would be embedded in the structure tangentially to the surface of the roll, allowing measurement of the contact friction. Another option is to utilize multi-axial force sensors in the place of singe axis force sensors used for the radial load measurement.

In the present study, a sweep of all the operating parameters was conducted in order to find the suitable operating parameter conditions. This led to situations where the bearing was overloaded and in contact with the roll. Furthermore, near the natural frequencies of the roll, the bearing was subjected to rather high excitations. As a result of the harsh conditions, there were some mechanical failures in the seal of the bearing. The authors suggest that the contact could have elevated the temperature of the seal leading to degradation of the adhesive. This, in combination with the high excitations led to the adhesive failing. In further studies, the seal could be instrumented with temperature sensors. Furthermore, the adhesive joint could be improved by introducing rough features to the sidewalls of the seal gum to form a mechanical bond between the restrictor and the gum in addition to the chemical bond. Finally, a higher operating temperature adhesive could be used.

The purpose of the present study was to validate the feasibility of the robust bearing concept. Thus, detailed uncertainty analysis has been omitted from the study. However, the quantitative results show feasibility in the concept after further investigations and optimizations.

CONCLUSION

In the present study, an implementation of a robust aerostatic bearing comprising of aerostatic seal and a pressure chamber was investigated. The investigated bearing was used to load a rotating paper machine roll in the radial direction. The performance of the seal was measured by measuring the load capacity, air consumption and the drive motor current of the roll.

The results of the present study showed that a maximum of 650 kg load could be transmitted from the bearing to the roll with negligible friction and leakage. At larger loads, there was intermitted contact between the bearing and the roll. The heat from the contact together with the higher amplitude vibrations near the natural frequency of the roll were severe enough to have a mechanical failure in the adhesive mounting of the restrictor to the seal body. In future work, the design of the bearing will be optimized to enable larger load capacity. Further, the manufacturing methods, especially the mounting of the restrictor to the seal body, will be investigated to improve the robustness of the bearing.

REFERENCES

[1] Roisum, D. R. (1996). *The mechanics of rollers*. Tappi Press.

[2] Gao, Q., Chen, W., Lu, L., Huo, D., & Cheng, K. (2019). Aerostatic bearings design and analysis with the application to precision engineering: State-of-the-art and future perspectives. *Tribology International*, *135*, 1–17. doi: 10.1016/j.triboint.2019.02.020

[3] Rasnick, W. H., Arehart, T. A., Littleton, D. E., & Steger, P. J. (1974). *Porous graphite air-bearing components as applied to machine tools*. available: https://www.osti.gov/servlets/purl/5110726

[4] Miettinen, M., Vainio, V., Theska, R., & Viitala, R. (2022). Aerostatically sealed chamber as a robust aerostatic bearing. *Tribology International*, *173*. doi: 10.1016/j.triboint.2022.107614

[5] J. Majuri, P. Sighn, M. Saksi, S. Tikka, P. Kuosmanen, and P. Kiviluoma, “Test equipment for curved aerostatic bearing”, P. Kiviluoma, P. Kuosmanen, and O. Tauno, Eds., Aalto University, 2022, pp. 23–28, ISBN: 9789526496153.

[6] R. Viitala, T. Widmaier, and P. Kuosmanen, “Subcritical vibrations of a large flexible rotor efficiently reduced by modifying the bearing inner ring roundness profile”,

Mechanical Systems and Signal Processing, vol. 110, pp. 42–58, 2018, ISSN: 10961216. doi: 10.1016/ j.ymssp.2018.03.010.

CONTACT

Valtteri Vainio	email:	valtteri.s.vainio@aalto.fi
Jaakko Majuri	email:	jaakko.majuri@aalto.fi
Petteri Haverinen	email:	petteri.haverinen@aalto.fi
Mikael Miettinen	email:	mikael.miettinen@aalto.fi
	ORCID:	https://orcid.org/0000-0002-9722-6756
Prof. Raine Viitala	email:	raine.viitala@aalto.fi
	ORCID:	https://orcid.org/0000-0003-1672-1921

